RARE EVENTS AND LOW PROBABILITY ERROR MODES IN AN ACTIVELY MODE-LOCKED LASER MODEL

G. M. DONOVAN* AND W. L. KATH†

Abstract. Modern optical communication devices and systems often have such low error rates that accurate study of these errors becomes difficult or impossible by traditional methods. We consider a soliton-based, actively mode-locked laser model with a very low error rate. In this model, errors are expected to occur in two different error "modes," referred to as "position slips" and "amplitude dropouts." Accurate and efficient Monte Carlo simulation of system performance and these error modes is obtained using importance sampling, made possible by the use of soliton perturbation theory. Furthermore, these two error modes are both shown to arise from a more general biasing problem for errors in the modeled system.

Key words. rare event simulation; monte carlo; importance sampling; solitons

AMS subject classifications. 35Q51, 35Q55, 65C05, 65C20, 78A40

1. Introduction. While mode-locked lasers are a technology dating back many years [1] and have been modeled extensively by many researchers (i.e. [2]), in recent years advances in the technology have allowed breakthroughs in many areas from optical frequency metrology [3] to optical clocks [4–6], breath analysis [7], communications [8], generation of high harmonics [9], measurement of fundamental constants [10] and possibly optical storage rings [11]. These applications are made possible by the very low error rates of the underlying laser systems.

One potential avenue of theoretical study of these systems is Monte Carlo simulation, which is frequently attractive in complex systems which can nonetheless be simulated numerically. Because of the high levels of performance obtained in these systems, and the correspondingly very low error rates, traditional or unbiased Monte Carlo simulation is often computationally infeasible because of the large number of trials required to accurately simulate rare events [12]. One approach to resolving this issue is a variance reduction technique known as importance sampling, which has been successfully applied to a number of problems in optical systems [12–19].

Importance sampling involves replacing the underlying probability distributions in the studied system with new, *biasing distributions*, under which previously rare events in the system (under the original distributions) are no longer rare. Generally speaking, determining these biasing distributions is the difficult aspect of employing importance sampling. While good biasing distributions can provide dramatic variance reduction and corresponding simulation speed-up, poor biasing distributions may instead make things worse.

For soliton-based systems, as the one we are considering, soliton perturbation theory provides a valuable tool for determining the biasing distributions [12]. The soliton modes, as well as the ODEs describing the soliton parameter evolution, allow us to pose a constrained optimization problem which can then be solved to obtain the biasing distributions. Using these biasing distributions in importance sampled Monte

*Department of Engineering Science and Applied Mathematics, Northwestern University, Evanston, IL, 60208, USA. Present address: Department of Mathematics, University of Auckland, Auckland 1142, New Zealand. email: g.donovan@auckland.ac.nz

†Department of Engineering Science and Applied Mathematics, and Northwestern Institute on Complex Systems, Northwestern University, Evanston, IL, 60208, USA. email: kath@northwestern.edu

Carlo simulations (ISMC), we are able to accurately simulate extremely rare events in this mode-locked laser system.

Furthermore, solving for the biasing distributions proves to be insightful in terms of the types of errors in the system. We first speculate that there are two, most-common types of error in the system, and are able to solve for the biasing distributions that generate these types of errors. However, posing a more general optimization problem results in families of biasing distributions which exhibit a bifurcation between the two expected error modes.

2. Model formulation. We model an actively mode-locked fiber laser as an optical cavity oscillator including an amplifier, filter, polarization rotator (and polarizer), and phase modulator. These elements introduce, respectively, (linear) gain, filtering, nonlinear gain (or loss), and phase modulation, in addition to the effects of optical propagation. The system under consideration is represented schematically by Fig. 2.1. Propagation through optical fiber is described by the nonlinear Schrödinger

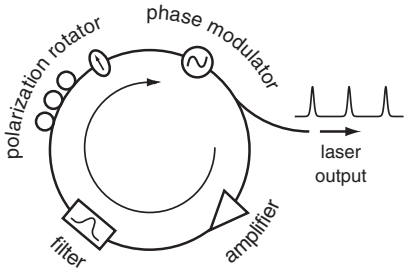

FIG. 2.1. *Schematic diagram of the simple mode-locked laser model, as an optical laser cavity including an amplifier, filter, polarization rotator and phase modulator.*

equation (NLS), which includes the dispersion and self-phase modulation effects inherent in optical fiber. The NLS is given by

$$\frac{\partial u}{\partial z} - \frac{i}{2}\beta\frac{\partial^2 u}{\partial t^2} - i\gamma|u|^2 u = -F(u,z,t) \tag{2.1}$$

where u is the optical field, β is the dispersion coefficient, γ is the nonlinear coefficient [20] and we have introduced in F perturbation terms to account for the other physical effects. Of course, in the absence of these perturbation terms, when $F \equiv 0$, Eq. (2.1) admits the well-known soliton solution

$$u_s(z,t) = E\,\mathrm{sech}(E(t-T-\Omega z))\exp\left(i\Omega(t-T)+i\phi\right) \tag{2.2}$$

arising from the balance between dispersion and nonlinearity. Here the soliton parameters E, T, Ω and ϕ correspond to the amplitude, position, frequency and phase of the soliton pulse, respectively. Note that the direction of propagation is z, with initial data $u(0,t) = u_0$ in the slow time coordinate.

To model the desired physical effects, we include the following terms in our perturbation F. First, we include the filtering cavity element with the frequency dependent gain (or loss) given by

$$a\frac{\partial^2 u}{\partial t^2}$$

where the parameter a is the filtering strength. The active phase modulation (mode-locking) is accomplished via

$$ib\cos(\omega t)u$$

where b is the modulation strength and ω is the external modulation frequency. Finally, the linear amplification gain is combined with the polarization rotator and polarizer in the form of a nonlinear gain term

$$c_1 u + c_2|u|^2 u + c_3|u|^4 u,$$

and Gaussian white noise is added at each pass through the gain medium ($z_n = nz_a$) so that the governing equation is then

$$\frac{\partial u}{\partial z} - \frac{i}{2}\beta\frac{\partial^2 u}{\partial t^2} - i\gamma|u|^2 u = \tag{2.3}$$
$$a\frac{\partial^2 u}{\partial t^2} + ib\cos(\omega t)u + c_1 u + c_2|u|^2 u + c_3|u|^4 u + \sum_{n=0}^{N} f_n(t)\delta(z - z_n).$$

Here the noise is described by

$$\langle f_i(t)\rangle = 0$$
$$\langle f_i(t) f_j^*(t')\rangle = \frac{(G-1)^2}{G\ln G}\frac{\eta_{sp}\gamma}{|\beta|}\delta(t-t')\delta_{ij}$$

and $\beta = 1.0$ ps^2/km, $\gamma = 1.0$ (km)$^{-1}$, $a = .002$ ps^2/km, $b = .01$ (km)$^{-1}$, $c_1 = -0.01$ (km)$^{-1}$, $c_2 = 0.034$ (km)$^{-1}$, $c_3 = -0.02$ (km)$^{-1}$, and the spontaneous emission factor η_{sp} is 1.25. The gain G exactly counterbalances the fiber loss $\alpha = 0.21$ dB/km. The governing equations are solved numerically via the split-step Fourier method [21] with 128 Fourier modes and a computational width of 30 ps, a propagation stepsize of $dz = 0.05$ km, and an initial soliton full-width half-max (FWHM) pulsewidth of 1.76 ps. The phase-modulation frequency is $\omega = 2\pi/25$ (1/ps).

3. Error modes & biasing distributions. In order to generate the biasing distributions needed for importance sampling in this system, we appeal to a reduced problem. By treating our modifications to the NLS and any deviations from the soliton pulse shape as small perturbations, we obtain evolution equations for the soliton pulse parameters. These evolution ODEs can then be used to formulate a boundary value problem (BVP), which can be solved to generate the biasing distributions and allow importance-sampled Monte Carlo simulations of the target system.

Consider a soliton pulse described by Eq. (2.2) and governed by Eq. (2.1), where the right-hand side is treated as a perturbation. The soliton parameter evolution equations can then be computed from

$$\frac{dE}{dz} = \mathrm{Re}\int_{-\infty}^{\infty} u^* F dt \tag{3.1}$$
$$\frac{d\Omega}{dz} = \frac{1}{E}\mathrm{Re}\int_{-\infty}^{\infty}(iu_t^* - \Omega u^*)F dt \tag{3.2}$$
$$\frac{dT}{dz} = \beta\Omega + \frac{1}{E}\mathrm{Re}\int_{-\infty}^{\infty}(t-T)u^* F dt \tag{3.3}$$

with the similar fourth equation for phase neglected in this phase-insensitive problem. By direct evaluation, we obtain the evolution equations for the soliton parameters E, T and Ω in differential form. The pulse frequency and position equations are given by

$$\begin{aligned} \frac{d\Omega}{dz} &= -A\Omega + B\sin(\omega T) \\ \frac{dT}{dz} &= \beta\Omega, \end{aligned} \tag{3.4}$$

where for clarity we assign $A = -\frac{4aE^2\gamma^2\Omega}{3\beta^2}$, and $B = \frac{b\omega^2\beta\pi}{2E\gamma}\mathrm{csch}\left(\frac{\beta\omega\pi}{2E\gamma}\right)$. Of course, these may be combined into a single, second-order governing equation

$$\frac{d^2T}{dz^2} + A\frac{dT}{dz} - \beta B\sin(\omega T) = 0, \tag{3.5}$$

describing a nonlinear oscillator for the soliton position parameter T.

Likewise, the evolution equation for the pulse energy is given by

$$\frac{dE}{dz} = 2(c_1 + a\Omega^2)E + \left(\frac{4c_2\gamma}{3\beta} - \frac{2a\gamma^2}{3\beta^2}\right)E^3 + c_3\frac{16\gamma^2}{15\beta^2}E^5. \tag{3.6}$$

The parameters c_1, c_2 and c_3 are set such that there are two stable energy states in the system. The first stable state corresponds to the desired, stable, nonzero pulse energy in the system. The second state is the zero state. The noiseless output from the laser is a series of fixed-length time intervals known as *bit slots*. In an *on-off keyed* (OOK) system, each bit slot would contain either a perfect soliton pulse ("on") or be identically zero ("off"). It is thus undesirable to have small amounts of energy in an otherwise empty bit slot grow into a pulse, and thus the zero energy state should be the second stable state.

In the system we have described thus far, we begin with the ansatz that there are two primary types of failure, or *error modes*, which occur. Understanding these error modes and their likeliness in given operating regimes is key to understanding the performance of the laser system, and to accurately simulating the rare error events involved.

One error mode is termed a *position slip*, in which a pulse shifts position (and/or frequency) so dramatically that it overcomes the phase modulation and "slips" into a neighboring bit slot. This error mode is illustrated schematically in the left panel of Fig. 3.1. In this case, our reduced problem guides us to the escape problem from the potential well created by the external phase modulation for pulse position, described by Eq. (3.5).

The other error mode we refer to as an *amplitude dropout*. In this case, the noise perturbations build up in the direction of decreasing amplitude and decrease the pulse energy past the crossover point into the stable state at zero energy. The pulse then disappears entirely into the zero-mean noise background. This error mode is illustrated schematically in the right panel of Fig. 3.1. This process is governed by the reduced problem given in Eq. (3.6).

4. Optimal biasing solutions.

4.1. Position slips. We now pose the problem for position slips only (ignoring the amplitude dropouts for now). We formulate the problem in terms of the addition of the product a *biasing coefficient* and the *adjoint mode* of the soliton to the signal to

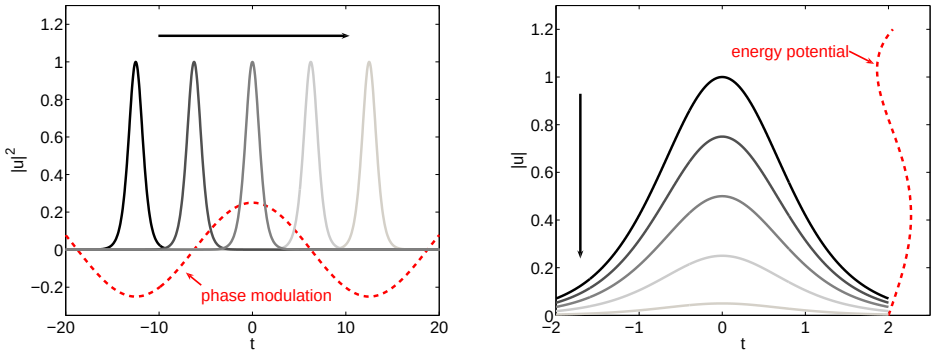

FIG. 3.1. *Left panel: cartoon of position slip error mode, with the phase-modulation potential (red, dashed) and a pulse moving from potential well to potential well. Right panel: cartoon of amplitude dropout error mode, with an energy potential overlaid on the vertical axis (red, dashed) and a pulse losing amplitude from its initial amplitude toward zero.*

produce the desired change in the soliton parameters in the most efficient (i.e. most likely) way, subject to the parameter evolution equations. It is not necessarily obvious that the adjoint soliton modes, as opposed to the direct, soliton modes give rise to the optimal solution. However, it can be shown that in fact it is the adjoint modes that lead to the most likely total changes in the corresponding soliton parameters [12]. Thus we will add the products of the biasing coefficients $\eta_\Omega(z)$ and $\eta_T(z)$ and the corresponding adjoint soliton modes $\underline{u}_\Omega(t)$ and $\underline{u}_T(t)$ along the path from $z = 0$ to $z = z_L$ such that starting from an initial position $T(z = 0) = T_0$ (corresponding to the noiseless soliton solution) we arrive at a prescribed value $T(z = z_L) = \hat{T}$. Here $\hat{T}$ is an error state, a result of a rare event in the system.

The biasing added to the solution, $\eta_\Omega \underline{u}_\Omega + \eta_T \underline{u}_T$, is a mean-shift of the additive Gaussian noise added at each pass through the gain media. Thus, our optimal solution, that which reaches the parameter target with the highest probability, is the solution which minimizes the total exponent

$$\int_0^{z_L} \left\{ \eta_\Omega^2(z) ||\underline{u}_\Omega||^2 + \eta_T^2(z) ||\underline{u}_T||^2 \right\} dz$$

subject to the differential equation side constraints

$$\begin{aligned} \frac{d\Omega}{dz} &= -A\Omega + B\sin(\omega T) + \eta_\Omega ||\underline{u}_\Omega|| \\ \frac{dT}{dz} &= \beta\Omega + \eta_T ||\underline{u}_T|| \end{aligned}$$

and the boundary conditions

$$\begin{aligned} T(0) &= T_0 \\ T(z_L) &= \hat{T} \\ \Omega(0) &= \Omega_0. \end{aligned}$$

The relevant modes are given by [22]:

$$\begin{aligned} \underline{u}_T &= E\tanh(E(t-T))u_s, \\ \underline{u}_\Omega &= -i(t-T)u_s. \end{aligned} \tag{4.1}$$

Here the primary constraint in terms of creating rare events is the final position $\hat{T}$. In a position slip, the pulse moves from its original position into a neighboring bit slot, i.e. $|T(z_L) - T_0| > \tau/2$, where $\tau = 2\pi/\omega$ is the bitslot width. Note that $\Omega(z_L)$ is unconstrained in this problem; this results in a natural boundary condition within the variational optimization problem [23]. Additional details for solving BVPs of this type are given in Sec. 5. Solving the resulting boundary value problem numerically, we obtain the continuous version of the biasing distributions for the optimal path from the fundamental soliton to the prescribed soliton parameter value $\hat{T}$. For fairly short total distances, the solution follows a simple path, rising monotonically toward the target value; for $z_L = 100$km, this solution is depicted in Fig. 4.1.

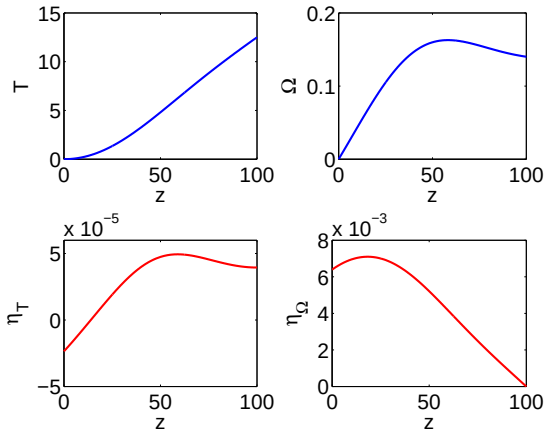

FIG. 4.1. *Optimal biasing path solution for the position slip error mode at $z_L = 100$ km. This optimal path is representative of the direct type of biasing path in the position slip error mode.*

However, when the total system length becomes longer, a new type of solution emerges, one with an oscillatory behavior. Recall that in the reduced system, the soliton position parameter T is governed by a damped nonlinear oscillator, Eq. (3.5). In this sense, then, it is unsurprising to see the oscillatory behavior of the optimal solution for $z_L = 600$km, with all other parameters unchanged, in Fig. 4.2.

Each of these biasing solutions allows us to generate a given portion of the pulse-position probability distribution function (PDF). Because we wish to simulate the entire PDF down to very low probability levels, we must use several biasing targets to encompass the entire region. Using family of solutions similar to Fig. 4.1 for $z_L =$ 100km and varying values of $\hat{T}(= T(z_L))$, we generate a group of biasing targets and combine the results using multiple importance sampling and the *balance heuristic* [24]. We then can use Monte Carlo simulation to generate a pulse position histogram and PDF ranging from the center of the bit slot far down into the tails, into neighboring bit slots. The results this simulation, along with the corresponding coefficient of

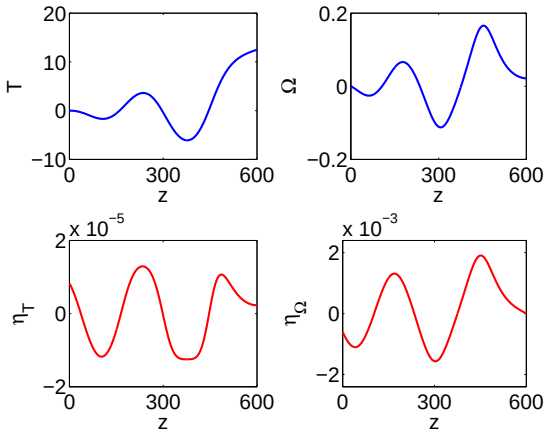

FIG. 4.2. *Optimal biasing path solution for the position slip error mode at $z_L = 600$ km. This optimal path is representative of the oscillatory type of biasing path in the position slip error mode.*

variation, are displayed in Fig. 4.3. The simulated PDF is reproduced periodically to illustrate the position overlap of pulses from neighboring bit slots.

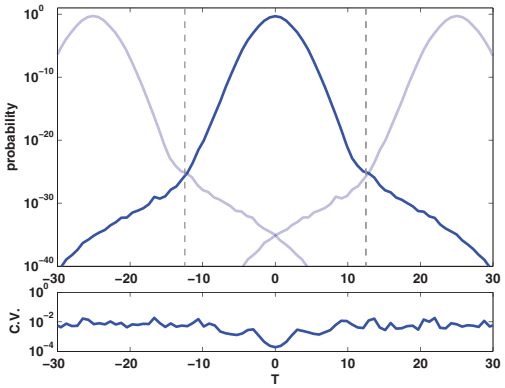

FIG. 4.3. *Simulated PDF for final pulse position. Neighboring PDFs are superimposed in light blue, and the bit slot boundaries at ±12.5 ps are indicated with dashed lines. The coefficient of variation, indicating the convergence level of the simulations, is displayed in the lower plot.*

4.1.1. Probability of exit from bitslot. The position-slip problem may also be viewed as an exit time problem – that is, what is the probability of a pulse at the equilibrium ($T = 0, \Omega = 0$) first escaping from the bitslot at a given distance z_L? The phase modulation creates an effective potential well from which the pulse must escape. For any given propagation distance, the optimal biasing problem can be solved for the most likely escape path. The ISMC process can be repeated, as before.

Unfortunately, as z_L increases the reduced problem begins to deviate significantly from the full nonlinear PDE, and simulation yields become intractably small, with very slow convergence. In Fig. 4.4, we give the results of the full ISMC simulations, up to $z_L = 500$ km. While for small values of z_L the simulations converge well with reasonable coefficients of variation, from approximately 200 km onward the c.v.

climbs unacceptably and the simulations no longer converge properly. This, of course, is always one risk when using ISMC.

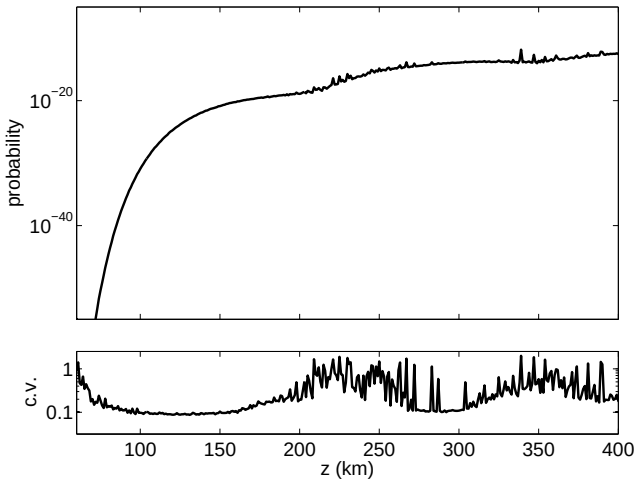

FIG. 4.4. *Simulated exit time for position slips, log-linear scale, resulting from 500,000 ISMC trials. Beyond* ~ 200 *km, the c.v. is too large and the simulations no longer converge sufficiently.*

In order to understand this failure, we examine individual pulse tracks from these simulations, compared with the optimal biasing solutions, for selected values of z_L in Fig. 4.5. In each panel, we compare the optimal biasing path (heavy black) with ten full simulations, using that biasing path. The simulations paths are colored red if they reach the target position, and grey if they do not. For small values of z_L (i.e., top panel), the simulation paths closely adhere to the optimal biasing solution, giving a high yield and good convergence of the simulations. As z_L increases (lower panels), the simulation paths begin to deviate significantly from the optimal biasing solution. This is the direct cause of the failure of the ISMC simulations to converge, and is also reflected in the sensitive dependence upon the boundary data in the biasing ODEs, which cannot be reliably solved by integration methods but instead by collocation [25]. Theory suggests that these tails, which cannot be captured numerically, should be asymptotically exponential [26, 27].

4.2. Amplitude dropouts. The same procedure can be performed for the other error mode, the amplitude dropout. Making use of Eq. (3.6) as the governing equation for the reduced problem, we reformulate the optimal biasing problem, but now with just one biasing parameter η_E controlling a single adjoint mode $\underline{u}_E$, subject to the constraint that the pulse amplitude parameter reaches a specified value, $E(z = z_L) = \hat{E}$. The relevant adjoint mode is given by [22]

$$\underline{u}_E = \frac{1}{E}\left(t - E(t-T)\tanh\left(E(t-T)\right)\right)u_s.$$

Observe that for this problem we will only be controlling the amplitude parameter, and thus we set $\Omega = 0$ in Eq. (3.6). The solution to this biasing problem, found numerically by collocation, for a single value of $\hat{E}$ is given in Fig. 4.6, again for $z_L = 100$km. Here the behavior does not change qualitatively as z_L varies, and this solution is typical.

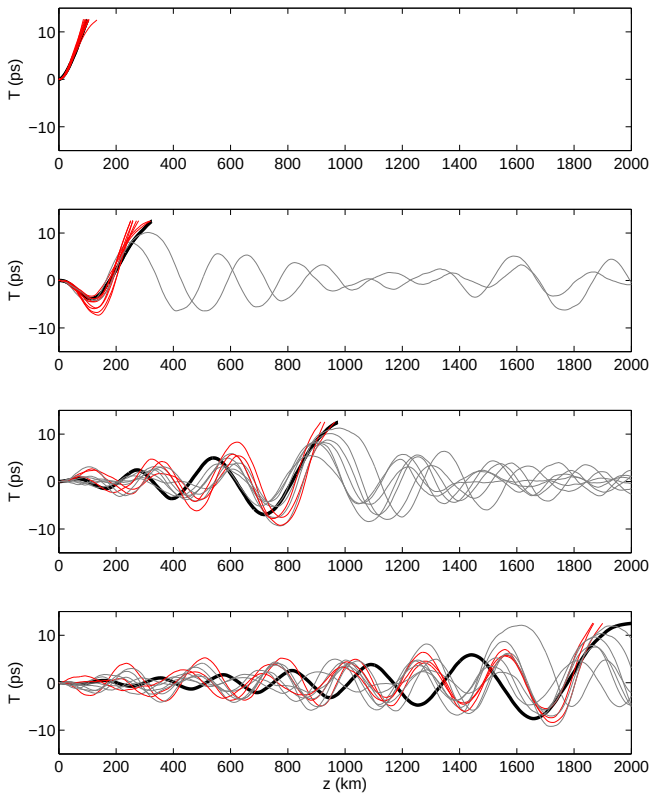

FIG. 4.5. *Comparison of optimal biasing and actual simulation paths. In each case, the heavy black curve is the optimal biasing path, beginning at $T = 0$ at $z = 0$, and "escaping" to $T = \hat{T} = 12.5ps$ at $z = z_L$. Each panel is for a single z_L, increasing from top to bottom. In each panel ten simulation paths are also given; those which reach the target value are colored red, and those which do not are grey.*

5. Combined biasing problem. Instead of treating each assumed error mode in isolation, we will now consider them together. To do so, we must consider and define a detector. The detector assigns a corresponding scalar value to the signal in each bitslot. One simple detector is the "amplitude detector", given by

$$I = \int_{-\tau/2}^{\tau/2} |u(z_L, t)|^2 dt.$$

This is simply the pulse energy integrated across the bit slot (or a fixed window) at the end of the transmission line. A decrease in this detected quantity can occur via either of the two error modes, but we need not restrict ourselves to one or the other. Instead, biasing for a decrease in this quantity with three of the adjoint modes (amplitude, position, and frequency – phase is irrelevant to this detector), we find expect to both error modes.

Now we have the biasing coefficients $\eta_\Omega(z)$, $\eta_T(z)$ and $\eta_E(z)$ and the corresponding

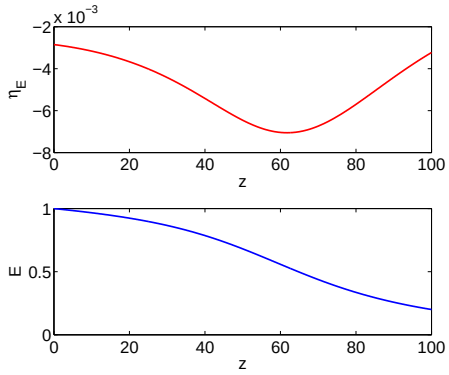

FIG. 4.6. *Optimal biasing path solution for the amplitude dropout error mode at* $z_L = 100$ *km.*

adjoint soliton modes $\underline{u}_\Omega(t)$, $\underline{u}_T(t)$ and $\underline{u}_E(t)$ along the path from $z = 0$ to $z = z_L$, such that starting from an initial position $I(z = 0) = I_0$ (corresponding to the noiseless soliton solution) we arrive at a prescribed value $I(z = z_L) = \hat{I}$. Here $\hat{I}$ is an error state, a result of a rare event in the system (i.e. a decrease in energy below the detection threshold).

The biasing added to the solution is $\eta_\Omega \underline{u}_\Omega + \eta_T \underline{u}_T + \eta_E \underline{u}_E$, and we minimize

$$\int_0^{z_L} \left\{ \eta_\Omega^2(z)||\underline{u}_\Omega||^2 + \eta_T^2(z)||\underline{u}_T||^2 + \eta_E^2(z)||\underline{u}_E||^2 \right\} dz$$

subject to the differential equation side constraints

$$\begin{aligned}
\frac{d\Omega}{dz} &= -A\Omega + B\sin(\omega T) + \eta_\Omega||\underline{u}_\Omega|| \\
\frac{dT}{dz} &= \beta\Omega + \eta_T||\underline{u}_T|| \\
\frac{dE}{dz} &= 2(c_1 + a\Omega^2)E + \left(\frac{4c_2\gamma}{3\beta} - \frac{2a\gamma^2}{3\beta^2}\right)E^3 + c_3\frac{16\gamma^2}{15\beta^2}E^5 + \eta_E||\underline{u}_E||
\end{aligned}$$

and the boundary conditions are

$$\begin{aligned}
T(0) &= T_0 \\
\Omega(0) &= \Omega_0 \\
E(0) &= E_0 \\
\int_{-\tau/2}^{\tau/2} |u(z_L,t)|^2 dt = E^2(z_L) \int_{-\tau/2}^{\tau/2} &\operatorname{sech}^2\left(E(z_L)[t - T(z_L)]\right) dt = \hat{I}
\end{aligned}$$

where the unconstrained boundaries again result in natural boundary conditions. Constructing the necessary functional with Lagrange multipliers $\lambda_{(1,2,3)}$ corresponding to the differential equation side-constraints for Ω, T and E respectively, and taking vari-

ations, we obtain the system

$$\begin{aligned}
\frac{d\lambda_1}{dz} &= \lambda_1 \frac{4aE^2\gamma^2}{3\beta^2} - \beta\lambda_2 + 4\lambda_3 aE\Omega \\
\frac{d\lambda_2}{dz} &= \lambda_1 \frac{\omega^3 b\pi\beta}{2E\gamma}\mathrm{csch}\left(\frac{\pi\beta\omega}{2E\gamma}\right)\cos(\omega T) \\
\frac{d\lambda_3}{dz} &= \frac{b\pi\beta\omega^2}{4E^3\gamma^2}\lambda_1 \sin(\omega T)\mathrm{csch}\left(\frac{\pi\beta\omega}{2E\gamma}\right)\left[-2E\gamma + \pi\beta\omega\coth\left(\frac{\pi\beta\omega}{2E\gamma}\right)\right] \\
&\quad + \frac{8\lambda_1 a\gamma^2}{3\beta^2}E\Omega - 2c_1\lambda_3 - 2\lambda_3\left(\frac{4c_2\gamma}{3\beta} - \frac{a^2\gamma^2}{3\beta^2}\right)E^2 \\
&\quad - \frac{16}{3\beta^2}\lambda_3 c_3\gamma^2 E^4 + 2\lambda_3 a\Omega^2 \\
\frac{d\Omega}{dz} &= -\frac{\omega^2 b\pi\beta}{2E\gamma}\mathrm{csch}\left(\frac{\pi\beta\omega}{2E\gamma}\right)\sin(\omega T) - \frac{4aE^2\gamma^2\Omega}{3\beta^2} + \frac{\lambda_1}{2} \\
\frac{dT}{dz} &= \beta\Omega + \frac{\lambda_2}{2} \\
\frac{dE}{dz} &= 2c_1 E + \left(\frac{4c_2\gamma}{3\beta} - \frac{2a\gamma^2}{3\beta^2}\right)e^3 + \frac{16c_3\gamma^2}{15\beta^2}E^5 - 2aE\Omega^2 + \frac{\lambda_3}{2}
\end{aligned}$$

which must be solved numerically to obtain the optimal biasing paths, for example using `AUTO` or `MATLAB`'s `bvp4c`.

By varying the target energy decrease $\hat{I}$, we find that there is a bifurcation in the optimal path through soliton parameter space to reach this target, with the branches corresponding to the two previously assumed error modes. This can be seen if Fig. 5.1, where the dashed line corresponds to the amplitude dropout mode, and the solid line to the position slip. In the left panel, the relative probability of each solution is given; in the right panel, the final position $T(z_L)$. For the position slip mode, the final position must be near $\tau/2$, while for the amplitude dropout mode, there is no change in position so $T(z_L) = T_0 = 0$. For small prescribed decreases in energy ($\hat{I}/I_0$ near 1), the most probable error mode is the amplitude dropout (dashed curve). As the required decrease in energy becomes larger ($\hat{I}/I_0 to 0$), the amplitude dropout becomes less probable, and eventually the position dropout becomes the preferred mode. The amplitude dropout mode always has a gradual descent in the detected quantity, as decreasing the pulse amplitude creates a corresponding drop in the detected quantity. However, the position slip has a different character – while initial changes in final position have little impact on the detected quantity, as the pulse is still largely within the integration window, when the body of the pulse reaches the edge of the integration window the detected quantity decrease per unit of biasing strength becomes very large at the margin. A small additional change in pulse position pushes a large amount of pulse energy outside of the detector window. The results of the numerical bifurcation solution are precisely in line with our qualitative expectations for the behavior of this system.

6. Discussion. We have shown that multiple importance sampling techniques based on soliton perturbation theory can be extended to be a useful tool for the study of rare events in mode-locked laser systems, of particular interest due to recent technical developments in optical frequency metrology which depend on high performance laser sources. This rare event simulation method allows fast and accurate simulation of these rare events and their statistics, which are simply unobtainable via traditional

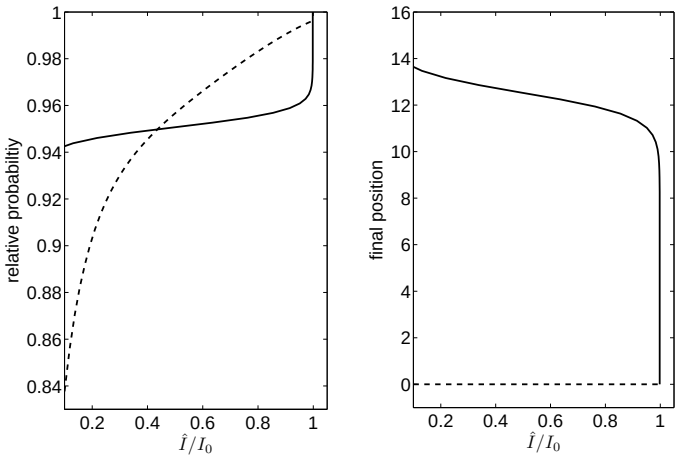

FIG. 5.1. *Diagram of the solution branches for the mode-locked laser system, where the solid line corresponds to the position slip error mode and the dashed line corresponds to the amplitude dropout. The relative probability of each solution (left) and the final pulse position $T(z_L)$ (right) are plotted against the relative energy decrease on the horizontal axis.*

Monte Carlo methods. While the method does depend critically on the mathematical structure of solitons, many laser systems do in fact use soliton or near-soliton pulses.

We have also shown that in addition to providing rare event simulation data for the system, this method also can provide interesting information about the types of errors in the underlying system – in this case, the position slips and amplitude dropouts. The combined biasing problem for any type of error in the system provides the expected transition between these error modes. While the model we have studied is a relatively simple choice, the method we have illustrated is shown to be highly effective should be applicable to more complicated and physically realized systems.

One limitation of this approach, particularly for OOK systems, is that we are unable to bias the "zeros" – that is, the bitslots which contain no pulse. Because the noiseless solution is trivial, there is no soliton to linearize about; treating this case is an open problem. There are of course other methods in the literature, for instance approaches based on assuming that the output distribution is Gaussian (though Fig. 4.3 is clearly not), or multi-canonical Monte Carlo (MMC) (i.e. [28–31]). While MMC has advantages, for example that it could be applied to non-soliton systems, it only produces the final output PDF and does not allow for exploring the importance of the error modes in the system.

References.

[1] W. E. Lamb. Theory of an Optical Maser. *Physical Review*, 134:1429–1450, June 1964.
[2] J. Nathan Kutz. Mode-locked soliton lasers. *SIAM Review*, 48(4):629–678, 2006.
[3] S. T. Cundiff. Metrology: New generation of combs. *Nature*, 450:1175–1176, December 2007.
[4] T. Udem, R. Holzwarth, and T. W. Hänsch. Optical frequency metrology. *Nature*, 416:233–237, March 2002.

[5] S. A. Diddams, J. C. Bergquist, S. R. Jefferts, and C. W. Oates. Standards of Time and Frequency at the Outset of the 21st Century. *Science*, 306:1318–1324, November 2004.

[6] J. Ye and S. Cundiff. *Femtosecond Optical Frequency Comb: Technology, Principles, Operation & Application*. Springer, New York, 2005.

[7] Michael J. Thorpe, David Balslev-Clausen, Matthew S. Kirchner, and Jun Ye. Cavity-enhanced optical frequency combspectroscopy: application to human breathanalysis. *Opt. Express*, 16(4):2387–2397, 2008.

[8] H. Haus. Mode-locking of lasers. *IEEE J sel top Q elec*, 6(6):1173, 2000.

[9] H. Kapteyn, O. Cohen, I. Christov, and M. Murnane*. Harnessing Attosecond Science in the Quest for Coherent X-rays. *Science*, 317:775–, August 2007.

[10] M. Fischer, N. Kolachevsky, M. Zimmermann, R. Holzwarth, T. Udem, T. W. Hänsch, M. Abgrall, J. Grünert, I. Maksimovic, S. Bize, H. Marion, F. P. Santos, P. Lemonde, G. Santarelli, P. Laurent, A. Clairon, C. Salomon, M. Haas, U. D. Jentschura, and C. H. Keitel. New Limits on the Drift of Fundamental Constants from Laboratory Measurements. *Physical Review Letters*, 92(23):230802–+, June 2004.

[11] K.L. Hall, J.D. Moores, K.A. Rauschenbach, W.S. Wong, E.P. Ippen, and H.A. Haus. All-optical storage of a 1.25 kb packet at 10 gb/s. *Photonics Technology Letters, IEEE*, 7(9):1093–1095, Sep 1995.

[12] RO Moore, G. Biondini, and WL Kath. A method to compute statistics of large, noise-induced perturbations of nonlinear schrödinger solitons. *SIAM Journal on Applied Mathematics*, 67:1418, 2007.

[13] R. O. Moore, G. Biondini, and W. L. Kath. Importance sampling for noise-induced amplitude and timing jitter in soliton transmission systems. *Opt. Lett.*, 28(2):105, 2003.

[14] G. Biondini, W. L. Kath, and C. R. Menyuk. Importance Sampling for Polarization-Mode Dispersion: Techniques and Applications. *Journal of Lightwave Technology*, 22:1201–+, April 2004.

[15] R. O. Moore, T. Schäfer, and C. K. R. T. Jones. Soliton broadening under random dispersion fluctuations: Importance sampling based on low-dimensional reductions. *Optics Communications*, 256:439–450, December 2005.

[16] E.T. Spiller, W.L. Kath, R.O. Moore, and C.J. McKinstrie. Computing large signal distortions and bit-error ratios in dpsk transmission systems. *Photonics Technology Letters, IEEE*, 17(5):1022–1024, May 2005.

[17] R. O. Moore, G. Biondini, and W. L. Kath. A method to compute statistics of large, noise-induced perturbations of nonlinear schr[o-umlaut]dinger solitons. *SIAM Journal on Applied Mathematics*, 67(5):1418–1439, 2007.

[18] J. Li, E. Spiller, and G. Biondini. Noise-induced perturbations of dispersion-managed solitons. *Physical Review A*, 75(5):053818–+, May 2007.

[19] G.M. Donovan and W.L. Kath. An iterative stochastic method for simulating large deviations and rare events. *SIAM Journal on Applied Mathematics*, 71:903, 2011.

[20] Govind P. Agrawal. *Nonlinear Fiber Optics*. Academic Press, 1995.

[21] T. R. Taha and M. J. Ablowitz. Analytical and Numerical Aspects of Certain Nonlinear Evolution Equations. II. Numerical, Nonlinear Schrödinger Equation. *Journal of Computational Physics*, 55:203–+, August 1984.

[22] A Hasegawa and Y Kodama. *Solitons in optical communications*. Oxford University Press, New York, 1995.

[23] I. M. Gelfand and S. V. Fomin. *Calculus of variations*. 1963. Revised English edition translated and edited by Richard A. Silverman.

[24] Eric Veach. Robust monte carlo methods for light transport simulation. *PhD thesis, Stanford University*, 1997.

[25] J. Galan-Vioque, B. Krauskopf, and H.M. Osinga. *Numerical continuation methods for dynamical systems: path following and boundary value problems; dedicated to Eusebius J. Doedel for his 60th birthday*. Springer, 2007.

[26] M. Williams. Asymptotic exit time distributions. *SIAM Journal on Applied Mathematics*, 42(1):149–154, 1982.

[27] M.I. Freĭdlin and A.D. Wentzell. *Random perturbations of dynamical systems*. Springer Verlag, 1998.

[28] Aurenice O. Lima, Ivan T. Lima, and Curtis R. Menyuk. Error estimation in multicanonical monte carlo simulations with applications to polarization-mode-dispersion emulators. *Journal of Lightwave Technology*, 23(11):3781, November 2005.

[29] Irina Nasieva, Andrey Kaliazin, and Sergei K. Turitsyn. Multicanonical Monte Carlo modelling of BER penalty in transmission systems with optical regeneration. *Optics Communications*, 262(2):246–249, June 2006.

[30] A. Bilenca, A. Desjardins, B. Bouma, and G. Tearney. Multicanonical Monte-Carlo simulations of light propagation in biological media. *Optics Express*, 13(24):9822–9833, November 2005.

[31] R. Holzlöhner and Curtis R. Menyuk. Use of multicanonical monte carlo simulations to obtain accurate bit error rates in optical communications systems. *Optics Letters*, 28(20):1894–1896, October 2003.